

**Differences in assigning probabilities to coastal inundation hazard estimators:
event vs. response approaches**

M. Sanuy^{1*}, J.A. Jiménez¹, M.I. Ortego² and A.Toimil³

¹Laboratori d'Enginyeria Marítima, Universitat Politècnica de Catalunya, BarcelonaTech, c/Jordi Girona 1-3, Campus Nord ed D1, 08034 Barcelona, Spain.

²COSDA-UPC. Applied Mathematics and Statistics Section of the Civil and Environmental Engineering Department., Universitat Politècnica de Catalunya, BarcelonaTech, c/Jordi Girona 1-3, Campus Nord ed C2, 08034 Barcelona, Spain.

³Environmental Hydraulics Institute “IHCantabria”, Universidad de Cantabria, Isabel Torres 15, 39011, Santander, Spain

* Corresponding author (marc.sanuy@upc.edu)

Abstract

Coastal flood risk assessment requires a reliable estimation of the frequency of inundation hazards, i.e. characterizing the hazard magnitude and assigning a probability of occurrence. In this work we analyse the uncertainty introduced in the assessment associated to the method to assign the probability of occurrence to coastal flood hazards. To this end we have compared the use of two general methods, the response and the event approaches. Different procedures are used to characterize coastal inundation hazards depending on the analysis scale and data availability. Thus, a range of possibilities has been analysed, from simple estimators such as run-up to modelled flood-prone areas. The analysis has been performed for all wave and water level

conditions around the Spanish coast. The results show that the differences between the methods are location-dependent, and thus, determined by the exposure to wave and water level conditions. When using the event approach, the run-up or total water level (with good correlation between waves and surge) distributions reasonably approximate those of the response approach with low associated uncertainty. When the assessment aims to output overtopping discharges or inundation maps, observed differences suggest that the event approach would produce misleading conclusions in inundation-related coastal management and decision-making.

Keywords

Run-up, total water level, overtopping discharge, inundation maps, EU Floods Directive, hazard indicators, uncertainty.

Introduction

Assessing the impact of coastal storms has become a global need motivated by the increasing number and value of assets located in coastal areas and the escalation of damages during the last decades (IPCC 2012, 2013). This is also true for the Spanish coast, where the same trend has been identified along its littoral front (e.g., Reyes et al. 1999; Rodriguez-Ramirez et al. 2003; Jiménez et al. 2012; Marcos et al. 2012, Toimil et al., 2017). Among the different storm-induced hazards, inundation is one of the most significant and damaging, and should be considered for its potential to increase in importance over the next decades (e.g., Jongman et al. 2012; Hinkel et al. 2014; Vousdoukas et al. 2018). The need for proper assessment of inundation is clear when designing coastal management plans, which will require a specific chapter on coastal risks as recognized in the protocol of Integrated Coastal Zone Management in the

Mediterranean (UNEP/MAP/PAP, 2008). The EU Floods Directive (EC, 2007) instructs management groups to prepare flood hazard maps for events of given probabilities of occurrence. Thus, the scientific community has developed multiple methodologies to assess storm-induced inundation through a variety of estimators (e.g., Sallenger 2000; Stockdon 2007; Ciavola et al., 2011a, 2011b; Tomás et al., 2016; Van Dongeren et al., 2018). Hazard-describing variables of multiple complexities can be used in inundation assessments to provide answers at both regional and local scales. Thus, the literature provides examples of regional parametric methodologies that scale hazard intensity using simple variables such as run-up, surge or total water level (e.g., hurricane impact at US coasts in Stockdon et al. 2007; storm impact along the Emilia-Romagna coast facing the Northern Adriatic described by Armaroli et al., 2012, and Armaroli and Duo, 2018; or storm impact in the northwestern Mediterranean coastline in Jiménez et al. 2018). Other approaches exist that assess the inundation at local (or even regional) scales using overtopping/overwash discharges or volumes as hazard estimators (e.g., Chini and Stansby, 2012) or by directly producing inundation maps (e.g., Prime et al. 2016), which can later be used to derive impacts by using receptor vulnerability data, and assess risks for decision support in coastal managing (e.g. Sanuy et al., 2018).

Considering both the nature of the forcing and processes controlling the coastal response, it is evident that inundation hazard assessment entails an inherent uncertainty in various parts of the analysis (e.g., Apel et al. 2004; Hall and Solomatine, 2008; de Moel et al., 2012), which should be studied to determine which of them are most influential in the final result and to efficiently utilize resources (e.g., Sayers et al., 2003). For instance, some studies assess the uncertainty associated with the method to identify the events (storms) or the extreme value distribution function selected for fitting (Arns et al., 2013, Winter et al. 2018). Uncertainty can be categorized into two

simple groups, i.e., the variability of nature (e.g. natural randomness of waves and surges) and the uncertainty of knowledge (e.g., numerical models, data analysis, etc). Prior to formal uncertainty analysis, an insight into the expected contributions associated with selected choices can be obtained by making a sensitivity assessment in which the same conditions are simulated when adopting such choices.

Within this context, the present study aims to quantify the sensitivity of inundation hazard assessments to the general scheme used to assign probabilities to hazard magnitudes. Two general methods will be compared, the so-called event and response approaches, since they are the two main conceptual schemes used in coastal hazard assessments to estimate probabilities or return periods (Garrity et al., 2006). This will be done with different hazard estimators from wave run-up to final inundation extension maps. The choice of the hazard-describing variable usually depends on the scale, objectives and available data of the studies. The choice of the method usually depends on the quantity and quality of the available data. In the event approach (EV), the starting points are pre-existing marginal distributions of waves and surges. Thus, the statistics are calculated based on the source in a univariate semi-deterministic mode. The response approach (RS) uses a large dataset (when available) of hydrodynamic data to both identify events and perform the statistical calculations directly based on the hazard target variables. The analysis for this work has been performed using a large dataset of 11 nodes around the Spanish coast and thus, covering the Cantabric, Atlantic and Mediterranean conditions. All nodes correspond to offshore data, and information on waves and surges are extracted at the same locations from the datasets. This includes the assessment of different wave and surge conditions to obtain results that help provide useful recommendations for different areas, which may be extrapolated to other domains with similar hydrodynamic characteristics.

Data description

To perform this analysis, data on waves, water levels and coastal morphology are required to characterize the forcing and the receptor respectively. Coastal inundation assessment requires continuous long-term availability of wave and sea level time series with adequate spatial and temporal coverage and such data must have been extensively checked and validated to prove their reliability. This work uses offshore wave and surge data obtained for a series of 11 locations along the Spanish coastal stretch covering the period from 1950-2014 (Figure 1).



Figure 1. Locations of wave and surge data used in this work. Data from the Global Ocean Waves (GOW, Reguero et al., 2012) and Global Ocean Surge (GOS, Cid et al 2014) were available for each node.

The offshore waves are obtained from the Global Ocean Waves (GOW) dataset (Reguero et al., 2012) which consists of a hindcast of hourly wave patterns with a spatial resolution of 0.0625° over a span of more than 60 years. These include the information on significant wave height and wave periods used in this work along with information on wave direction and wave spreading. GOW was simulated with the WaveWatchIII model (Tolman et al., 2002) and driven by the NCEP SeaWind I winds (Menendez et al., 2014). The meteorological sea-level component comes from the Global Ocean Surge 1.1 (GOS1.1) database (Cid et al. 2014). GOS1.1 was developed using the Regional Ocean Model System (ROMS) of Rutgers University and forced with NCEP SeaWind I winds, which provided an hourly-basis hindcast of surge levels with a spatial resolution of 0.125° between 1948 and 2014. Both datasets have enough resolution and accuracy to describe the coastal processes at all locations which has been verified using historical records from buoys, tide gauges and open-ocean satellite observations (Reguero et al., 2012 and Cid et al., 2014).

Since the magnitude of storm-induced flooding depends on the coastal characteristics, we used different types of data to characterize a representative morphology. Thus, on the one hand, for cross-shore inundation estimators (e.g., Ru, overtopping discharges/volumes), the coast is synthetically represented by different beachface slopes covering dissipative to reflective conditions in the range of 0.025 to 0.2 and elevations from 1.5 to 5 m above mean water level. On the other hand, to illustrate the effects on inundation extent, we selected a low-lying flood-prone area, which is represented by the topography of the Tordera Delta in the northwest Mediterranean (see e.g., Jiménez et al. 2018). Topographic data were derived from a

LIDAR flight performed in 2010 with a 1×1 m resolution and a vertical error of 6 cm provided by the Catalan Cartographic and Geologic Institute.

Methodology

The methods used at the different steps of the inundation hazard assessment are presented as follows. First the variables used to estimate the inundation hazard and compare the event and response approaches are presented. Second, the statistical methods used to select storms and for the extreme value analysis are introduced. Third, the general framework of the event and response approach is presented followed by the clustering method used to group datasets from the obtained results, and the description of the comparative methodology.

Inundation hazard estimators

The inundation hazard-describing proxies analysed in this work are the wave-induced run-up (Ru), the total water level at the beach (TWL), the overtopping discharge (Q), the total water volume flowing into the hinterland (TWV) and the inundation maps.

Wave Ru is an important parameter to properly characterize storm-induced coastal inundation and can be used as a hazard estimator to assess coastal vulnerability to flooding in regional-scale approaches (Bosom and Jiménez, 2011; Ferreira et al. 2017; Jiménez et al. 2018). The accurate prediction of Ru is difficult given the complexity of the processes involved such as the energy dissipation in the surf zone and the interactions between the infragravity and incident wave bands (Ruggiero et al. 2004). There are a number of models that have been derived or specifically calibrated to be applied to beaches (e.g., see Mather et al., 2011). In this work, we use the formula proposed by Stockdon et al. (2006), which has been specifically derived from a large

dataset of Ru values measured in field experiments covering different beach characteristics. It is extensively used as a Ru model for open sedimentary coasts and it predicts the $Ru_{2\%}$ magnitude as:

$$Ru_{2\%} = 1.1 \left(0.35 \tan \beta (H_s L_o)^{1/2} + \frac{[H_s L_o (0.563 \tan \beta^2 + 0.004)]^{1/2}}{2} \right), \quad (1)$$

and under extremely dissipative conditions ($\xi_o < 0.3$) by:

$$Ru_{2\%} = 0.043 (H_s L_o)^{1/2}, \quad (2)$$

where H_s is the deepwater significant wave height, L_o is the deepwater wave length associated with the wave peak period (T_p), $\tan \beta$ is the beachface slope, and ξ_o is the Iribarren number, which is given by

$$\xi_o = \frac{\tan \beta}{\sqrt{H_s/L_o}}. \quad (3)$$

Wave induced run-up is usually combined with the storm surge (SU) to derive the TWL at the beach. This corresponds with the stochastic component of the water level and omits the astronomical tide. The TWL is also commonly used as an estimator in coastal inundation assessments when the incidence of the surge component is important (e.g., Benavente et al. 2006, Stockdon et al 2007, Armaroli and Duo, 2018).

When the TWL is significantly higher than the beach elevation, overwash and/or overtopping will occur and this will determine the total volume of water entering into the hinterland. Overtopping (Q) depends on the freeboard during the event, defined as the vertical height of the beach or coastal structure above the still water level, and the level reached by the wave-induced Ru (Pullen et al., 2007).

Different formulations exist to obtain this flow rate from the given wave conditions, and most of them were developed to characterize overtopping at seawalls and breakwaters (see Pullen et al., 2007). In this work, the overtopping discharge Q was evaluated using the semi-empirical model proposed by Hedges and Reis (1998) (hereinafter denoted as H&R) with the coefficients A and B given by Reis et al. (2008):

$$\frac{Q}{\sqrt{gR_{\max}^3}} = \begin{cases} A \left(1 - \frac{Rc}{\gamma_r R_{\max}}\right)^B & 0 \leq \frac{Rc}{\gamma_r R_{\max}} < 1 \\ 0 & \frac{Rc}{\gamma_r R_{\max}} \geq 1 \end{cases}, \quad (4)$$

where R_{\max} is the maximum wave run-up value during the storm, γ_r is a roughness coefficient ($\gamma_r = 1$ for sand) and Rc is the beach freeboard relative to still water level.

Analogously to the analysis performed by Laudier et al. (2011), eq.1 and 2 are used to estimate the wave Ru which feeds eq.4 after proper transformation.

Once the water levels are known and the flood discharge is calculated, the total water volume (TWV) entering the hinterland during the event can be calculated. This was done by directly integrating each discharge over the time-step (without consideration of the percentage of overtopping waves) and by addition of time-steps over the duration of the storm. This volume can then be used to compute the extension of the inundation of a given area. In this work, we used the raster-based LISFLOOD-FP inundation model, which has been successfully employed to simulate inundations in fluvial and coastal areas (Bates and de Roo, 2000; Bates et al., 2005). The model is used to propagate discharges into the hinterland, and thus, to provide an estimation of the inundation extension over a low-lying flood-prone area given the magnitude of the discharges along the beach. LISFLOOD-FP treats floodplain flows using a storage cell approach first developed by Cunge et al. (1980), which is implemented for a raster grid to allow

an approximation for 2D diffusive wave and momentum equations for each direction. In this model, the flow between cells is calculated according to Manning's law. The model predicts water depths in each grid cell at each time step and simulates the dynamic propagation of waves over the floodplain. The grid is formed by $3 \text{ m} \times 3 \text{ m}$ cells obtained from the existing LIDAR, i.e. the original $1 \text{ m} \times 1 \text{ m}$ LIDAR data has been resampled to reduce the computational time while maintaining a high-resolution grid. In this study, a constant value for the Manning's roughness of 0.06 is used throughout the floodplain, according to the recommendations of Arcement and Schneider (1989) for this type of surface i.e., moderate degree of irregularity, minor obstructions and medium to large vegetation.

Storm selection and extreme event probability distribution

In this work, the Peak Over Threshold (POT) approach (see e.g., Coles, 2001; Dupuis, 1998) is used to identify extreme events with a double threshold approach. First, the 98 percentile of the time series (either H_s , SU , Ru or TWL) was used considering only events with durations over 6 h and imposing a 72 h time gap between events to ensure independence. Thus, the first threshold controls the duration of the events and the time of fair-weather conditions between them. Later, the 99.5 percentile is used as the criterion for minimum value at the peak of the event (i.e., only events exceeding the second threshold at the peak are considered extreme).

This approach was adopted to obtain storms in terms of H_s and SU for the event approach (Table 1) from the GOW and GOS datasets at the 11 selected nodes. For the response approach, the POT is applied to the Ru and TWL variables previously calculated for the whole length of the datasets (following scheme in Figure 2). The double threshold ensures homogeneous statistical criteria to locate extreme events

across datasets and has been designed for an output average of ~4-6 events per year. The lower threshold (98 percentile) matches, as a reference, the magnitude of Class 1 events (low energy content) according to Mendoza et. al (2011) for northwest Mediterranean storms (nodes 8 to 11, Table 1).

Table 1. Values of the 98 and 99.5 percentiles used as thresholds at each node for all variables under the POT approach and the number of obtained storms per site and variable from 1960 to 2014.

Node	Hs (m)			SU (m)		
	98%	99.5%	n° storms	98%	99.5%	n° storms
1	3.67	4.24	231	0.25	0.29	180
2	4.44	5.12	229	0.26	0.31	162
3	6.65	7.53	231	0.27	0.32	155
4	6.49	7.28	226	0.24	0.28	163
5	3.21	3.81	187	0.18	0.22	170
6	2.66	2.99	252	0.21	0.25	84
7	2.65	3.01	316	0.19	0.23	145
8	2.55	2.98	268	0.20	0.24	153
9	2.40	2.87	246	0.23	0.27	121
10	2.58	2.99	271	0.24	0.28	132
11	2.57	3.08	253	0.24	0.28	174

To assign probabilities to the obtained events, an extreme value distribution was fitted to the data. In this work, the Generalized Pareto Distribution (GPD) is used for that purpose (Davison and Smith, 1990). GPD is given by ($\sigma > 0$ and $y > 0$):

$$F_Y(y; \sigma, \xi) = 1 - \left(1 + \frac{\xi}{\sigma} y\right)^{-\frac{1}{\xi}}, \quad (5)$$

where ξ and σ are the shape and scale parameters. The GPD has three domains of attraction, which are $\xi < 0$, $\xi = 0$ and $\xi > 0$ and represent the Weibull (upper-bounded), Gumbel (exponential) and Fréchet (heavy tailed) domains, respectively. Following Egozcue et al. (2006), the storm data is log-transformed before fitting the GPD. Thus, in

eq.5, $y = \log(X-u)$ and u is the 99.5 percentile threshold (Table 1). The log-scale represents an improved method for positive measurements in which the differences are relative (Tarantola 2006). All of the considered variables in this work describe physical processes that are upper-bounded, and therefore a GPD-Weibull is a suitable model for them.

Table 2 presents the fitted parameters for the Hs, SU, Ru and TWL extreme value distributions, along with the modified Anderson-Darling Statistic A^* (Stephens, 1977) which illustrates the goodness of fit as follows: at a significance level α of 0.01, the GPD is accepted as a good fit for the data for A^* values lower than 1.04. As it can be observed, most of the data is correctly represented with a GPD with the following considerations: node 7 presents A^* values slightly above the acceptance threshold for all tested variables, and the GPD is less representative for the SU data at most of the Mediterranean locations (nodes 6 to 10). However, it is considered that GPD fits the datasets correctly enough to perform the comparison between event and response methodologies.

Table 2. Fitted scale (ξ) and shape (σ) parameters for the Hs, SU, Ru and TWL extreme value distributions. The modified Anderson-Darling Statistic A^* (Stephens, 1977), denotes a good fit for values lower than 1.04 (at alpha level 0.01).

	Hs			SU			Ru (slope 0.1)			TWL (slope 0.1)		
	ξ	σ	A^*	ξ	σ	A^*	ξ	σ	A^*	ξ	σ	A^*
node 1	-0.37	0.11	1.17	-0.25	0.10	0.88	-0.37	0.09	0.13	-0.35	0.09	0.31
node 2	-0.38	0.11	0.58	-0.28	0.10	0.17	-0.38	0.09	0.49	-0.41	0.10	0.40
node 3	-0.42	0.11	0.35	-0.44	0.13	0.57	-0.38	0.08	0.57	-0.37	0.08	0.88
node 4	-0.38	0.10	0.63	-0.43	0.13	0.43	-0.28	0.07	0.49	-0.31	0.08	0.45
node 5	-0.36	0.12	0.33	-0.51	0.16	0.21	-0.26	0.10	0.26	-0.26	0.11	0.38
node 6	-0.16	0.08	0.43	-1.04	0.37	4.66	-0.19	0.08	0.79	-0.20	0.08	0.97
node 7	-0.20	0.09	2.01	-0.54	0.20	4.19	-0.15	0.08	1.46	-0.16	0.08	1.62
node 8	-0.20	0.11	0.50	-0.49	0.18	3.67	-0.14	0.08	0.19	-0.16	0.09	0.25
node 9	-0.31	0.14	0.24	-0.55	0.21	6.87	-0.22	0.10	0.30	-0.26	0.11	0.20
node 10	-0.32	0.13	0.48	-0.51	0.19	5.23	-0.24	0.10	0.52	-0.28	0.11	1.16
node 11	-0.29	0.12	0.36	-0.34	0.13	0.23	-0.22	0.09	0.22	-0.27	0.10	0.34

Regarding the Q and TWV parameters, the GPD presents poorer goodness of fit results specially for slope-freeboard combinations giving a low number of storms producing discharges and due to the nature of eq.4. In order to include only those cases with better fittings, only combinations with more than one storm per year producing discharges are included in the final comparison assessment.

The event and response approaches

In coastal inundation assessments, two main approaches exist to assign probabilities or return periods to hazard magnitudes, which are commonly known as the event and response methods (Garrity et al., 2006); the method to be used will usually be imposed by the available initial data.

çThe event approach (EV) (Figure 2) is a semi-deterministic methodology, where the starting point is determined by the extreme probability distribution of wave heights and storm surges in addition to some empirical relationships with other storm parameters of interest such as wave period and storm duration. When these are the only available data, it must be assumed that the hazard variables of interest (Ru, TWL, Q, TWV or the inundation map) have the same probability of occurrence than the forcing (wave and storm surge).

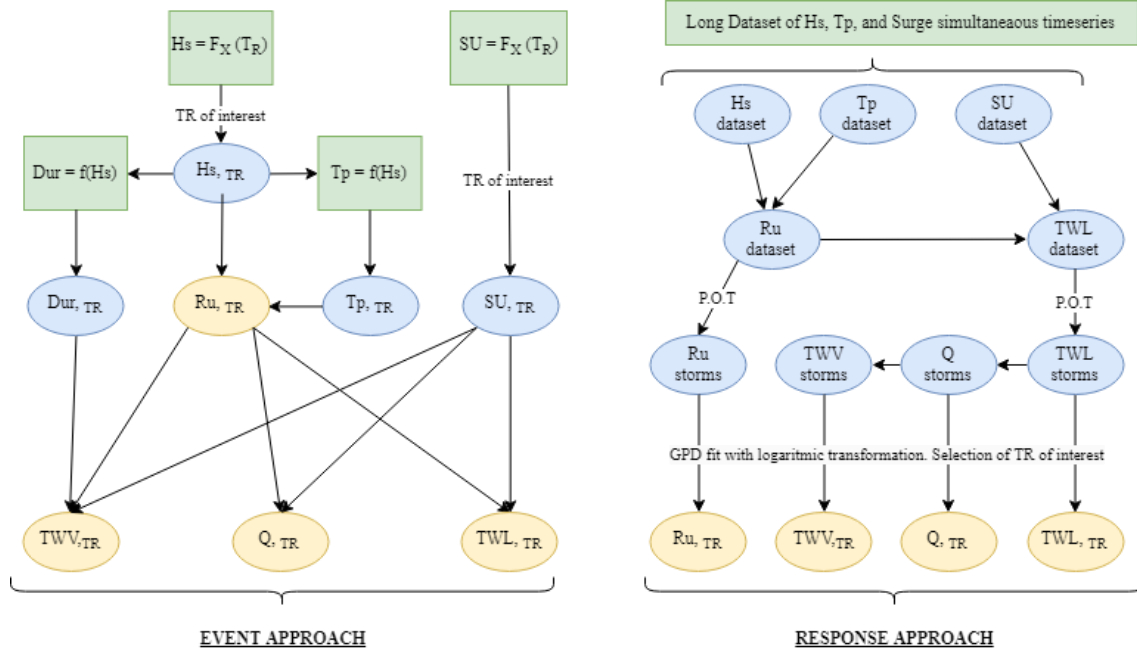


Figure 2. A flow chart of the steps and their interdependencies in the analysed methods: event (EV) and response (RS). $F_X(TR)$ represents the extreme distribution and $f(Hs)$ the deterministic relationships of a variable with the wave height.

In this work, the starting point of the EV corresponds to the fitting of marginal Hs and surge extreme distributions at all nodes (Figure 2, Hs and SU as $F_X(TR)$; Figure 3-a and b). This starting point is usually available in a pre-processed way and provides wave height and storm surge values for a given return period of interest (TR) (Figure 2). The remaining parameters required to fully characterize the event, i.e., wave period and storm duration, are calculated by using deterministic relationships (Figure 2, $Tp = f(Hs)$ and $Dur = f(Hs)$; Figure 3-c and d), since the use of EV is usually imposed by the lack of available data to perform bivariate statistical approximations (as in e.g. Lin-Ye et al. 2016). With this approach each wave height is associated with just one value of the other storm parameters. This implies the loss of significant information regarding the natural variability of the processes (Sánchez-Arcilla et al., 2009, Masina et al., 2015).

Obtained R_u is combined with the SU of the same TR of interest to get the TWL (by addition) or Q (with eq.4). This is the simplest and most conservative application of the event approach corresponding to situations in which simultaneous datasets of interest are not available. In other cases, bi(multi)-variant statistical distributions could be calculated (e.g., Hawkes et al. 2002, Masina et al. 2015, Lin-Ye et al. 2016), but this would imply that a large dataset is available and therefore the response approach could be applied as well. In order to estimate discharge evolution during the storm (e.g., to produce inundation maps or to integrate discharges into TWV), an assumption about the shape of the storm development in time must be made. One of the most common hypotheses is imposing a triangular shape with the peak of the event at the centre of the duration (McCall et al. 2010, Poelhekke et al. 2016); therefore, it is the one adopted here to derive deterministically TWV and inundation maps for the event approach.

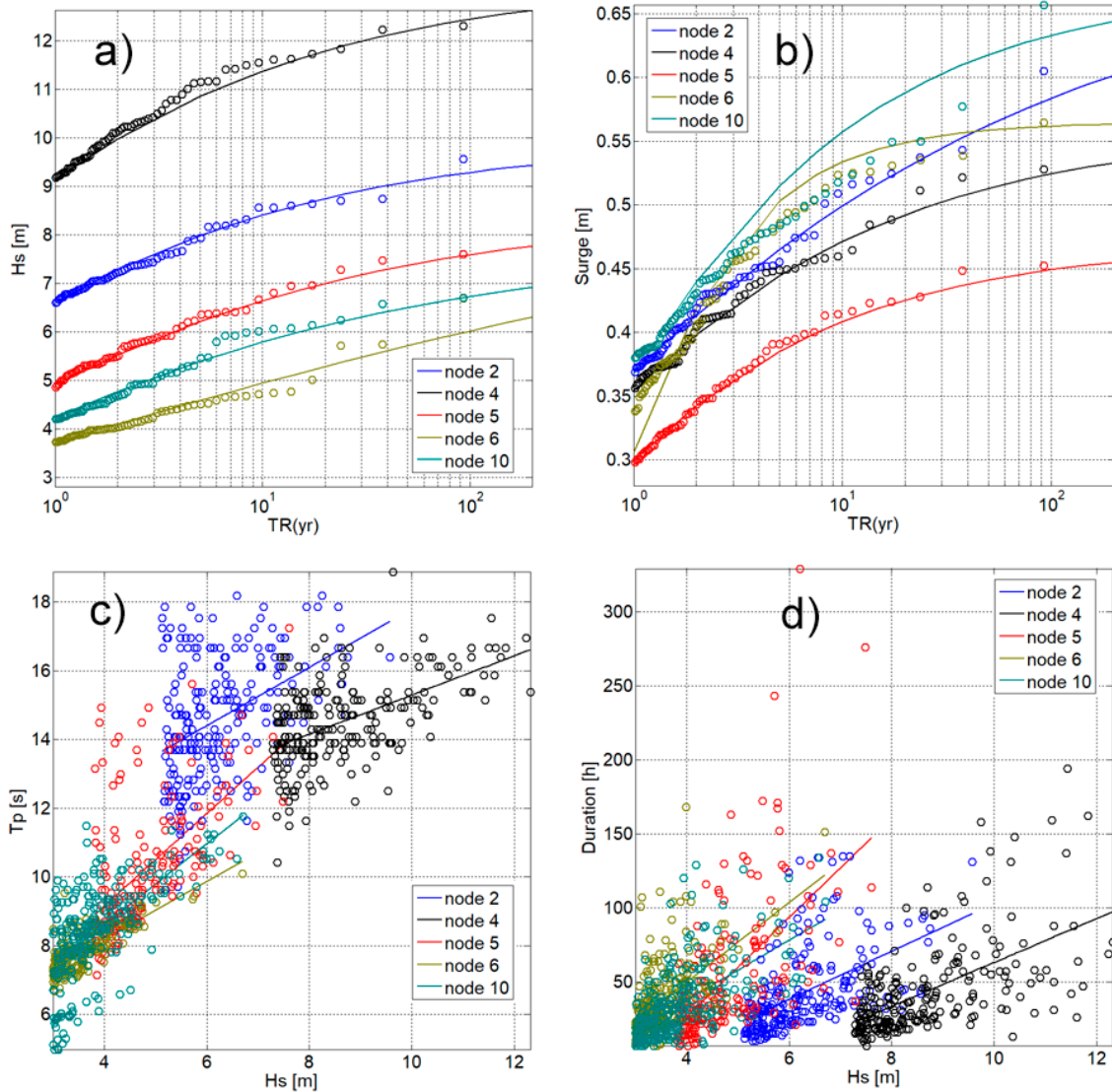


Figure 3. Extreme distributions of H_s (a) and SU (b). T_p vs H_s (c) and duration vs H_s (d) relationships for representative nodes covering the different conditions along the Spanish coast (2-Cantabric, 4-N. Atlantic, 5-S. Atlantic, 6-S. Mediterranean and 10-N. Mediterranean)

In the response approach (RS), the entire original wave and water level time series are used to establish the hazard parameters of interest. Thus, Ru datasets in all 11 locations are calculated from the available H_s and T_p time series. These are combined with simultaneous SU data to obtain the TWL time series. Then, the POT method is used on

both Ru and TWL datasets to identify storms in terms of the target estimator. This permits the proper inclusion in the assessment of the natural variability associated with the simultaneous occurrence of the involved variables without imposing any assumption. From the TWL storm dataset, Q time series and integrated TWVs can be calculated for each event without assumptions on the events' durations and shapes. The response method is especially recommended when wave variables during storms (e.g., Hs, Tp and duration) are poorly or partially correlated and it is recommended by the FEMA guidelines for flooding studies (Divoky and McDougal, 2006). However, it can only be applied if long records (either simulated or measured, covering many years) of the involved variables are available.

Figure 4 shows an example of the so-obtained extreme distributions of inundation hazard estimators following both approaches for representative nodes along the Spanish coast. The differences in shape of the Q and TWV distributions (Figure 4, c-d) are caused by the properties of eq.4, and the fact that in the EV approach these are deterministically calculated from the TWL distribution (Figure 4, b), while in the RS method a GPD is fitted to maximum Q at the peak and TWV of each storm.

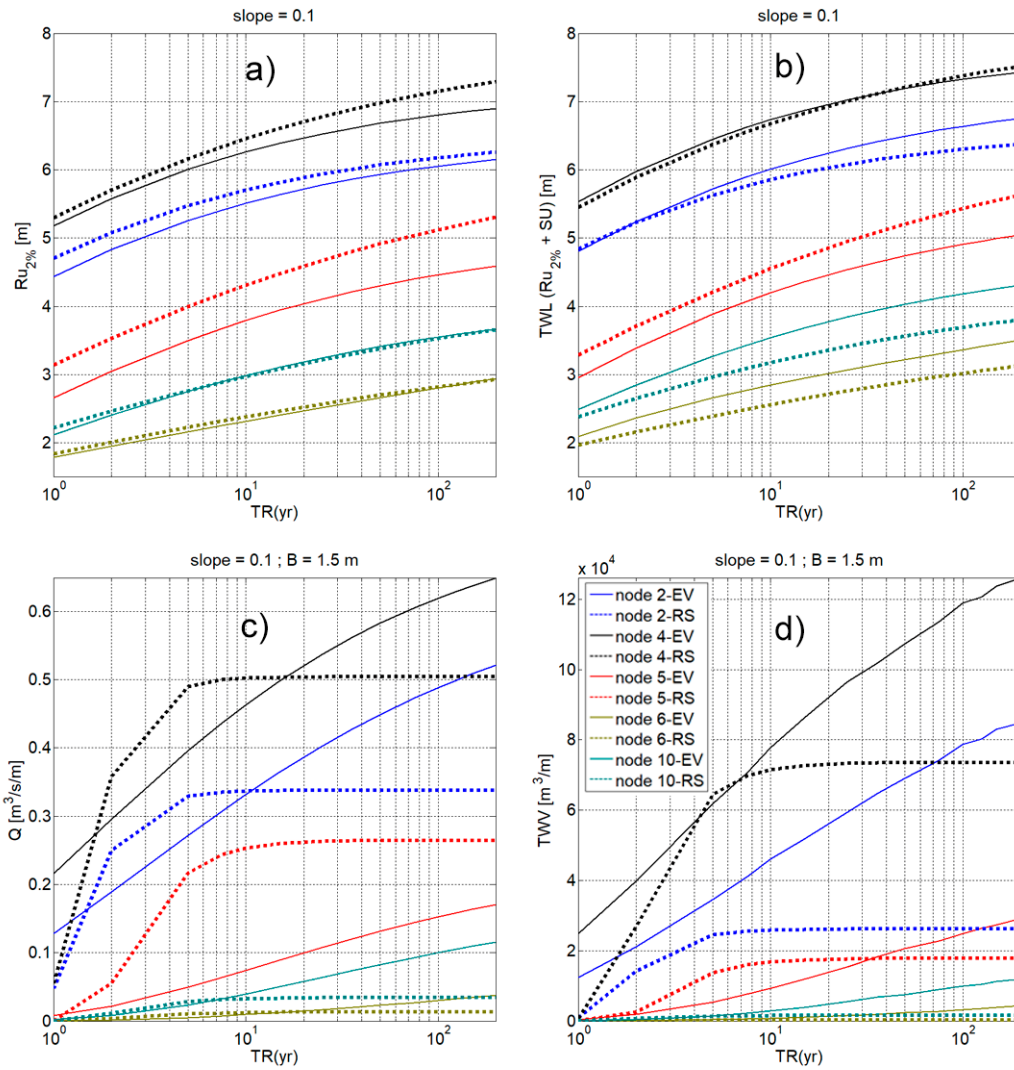


Figure 4. Examples of method comparison results for the selected locations (2-Cantabric, 4-N. Atlantic, 5-S. Atlantic, 6-S. Mediterranean and 10-N. Mediterranean) and morphologies (slope = 0.1 and $B = 1.5$). The selected datasets are presented to illustrate the absolute magnitudes of the involved variables at each of the main oceanic fronts.

Comparative assessment and clustering

The results are calculated at reference return periods (5, 10, 25, 50, 100 and 150 years) for each estimator (Ru, TWL, Q, and TWV), location (node) and approach (EV and RS). The relative differences between EV and RS approaches were calculated as

$$Diff\% = \frac{RS_{variable} - EV_{variable}}{RS_{variable}} * 100 \quad (6)$$

The Ru and TWL variables were assessed for different slopes (0.025, 0.075, 0.1, 0.14, and 0.2). These are hypothesized slopes that can be present at all 11 locations, except for 0.025, which is characteristic of some deltaic environments. The relative differences in terms of Ru and TWL (per return period and slope) were used as baseline to perform a cluster analysis. The selected clustering method was the inner squared distance (minimum variance algorithm). The aim was to group the 11 locations in representative clusters according to similarities in their differences between EV and RS approaches by using two variables including the wave and surge variabilities at each node (Figure 5).

For each variable, the results from all locations within clusters, slopes and freeboards, are integrated by calculating the median of the relative differences, and the 95% probability interval given by the 0.025 and 0.925 quantiles (Figures 6, 7 and 8).

The Q and TWV variables were assessed for slopes higher than 0.05 since this is the lower limit to apply the H&R model according to Reis et al. (2008). Thus, the considered slopes were (0.075, 0.1, 0.14, and 0.2). For each slope, different beach heights were tested ranging from 1.5 m to 4 m with 0.5 m steps. If a combination slope-height was observed to cause less than one discharge event per year, it was not included in the result integration (Figures 7 and 8).

Results

Spatial Clustering

The obtained dendrogram (Figure 5) of the cluster analysis highlights 4 main groups with differentiated behaviour. The analysis clearly detects 2 big groups corresponding to the Atlantic and Cantabric coasts (nodes 1 to 5) and the Mediterranean Sea (nodes 6 to 11).

Each group is divided into two clusters where different trends of Ru and TWL differences are detected. The area corresponding to the Gulf of Cadiz (CAD, node 5) is clearly differentiated from the rest of N. Atlantic and Cantabric locations (AT-C, nodes 1 to 4). At the Mediterranean front, nodes 8 and 10 are grouped in a different cluster but with higher similarity than the division at the Atlantic-Cantabric front. Hereinafter, the analysis is done by comparing the results for the four clusters.

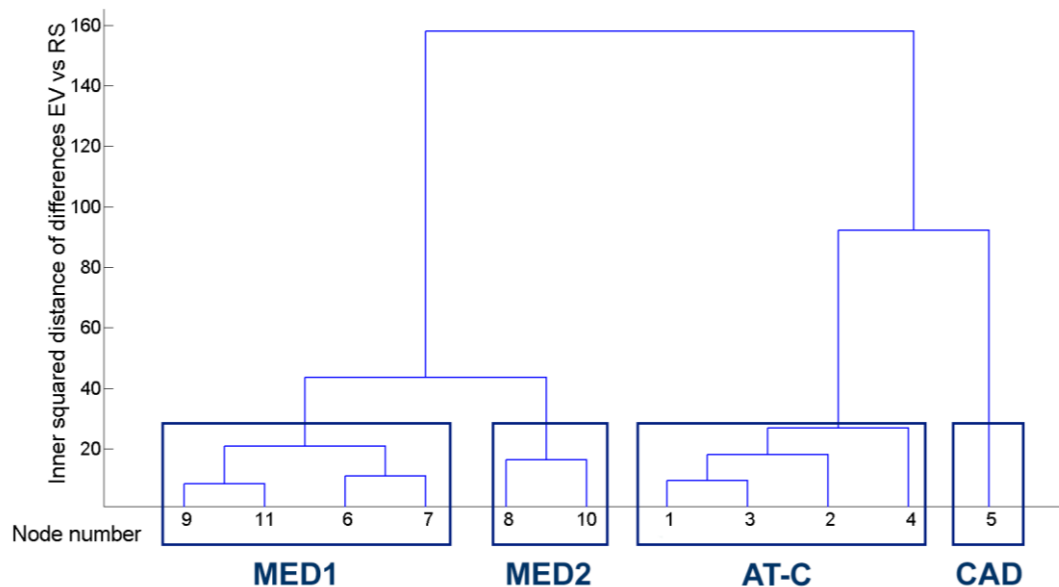


Figure 5. Dendrogram of the 11 locations based on Euclidean distance in terms of run-up (Ru) and total water level (TWL). Mediterranean locations (MED1 and

MED2) are separated from N.Atlantic-Cantabric locations (AT-C) and Gulf of Cadiz (CAD).

Water level estimators

Figure 4 shows the obtained extreme distributions of Ru and TWL for representative nodes of each cluster. As expected, the magnitude of Ru is almost double for AT-C locations (nodes 1 to 4) than for MED1 and MED2 nodes (nodes 6 to 11).

However, when the relative differences in Ru between approaches are analysed, results show that in all locations except for node 5 (CAD), values are low and mainly contained in the 0-5% (Figure 6). Notably, at CAD differences are ~10% and can go up to 20% for low slopes and high return periods (100-150 yr).

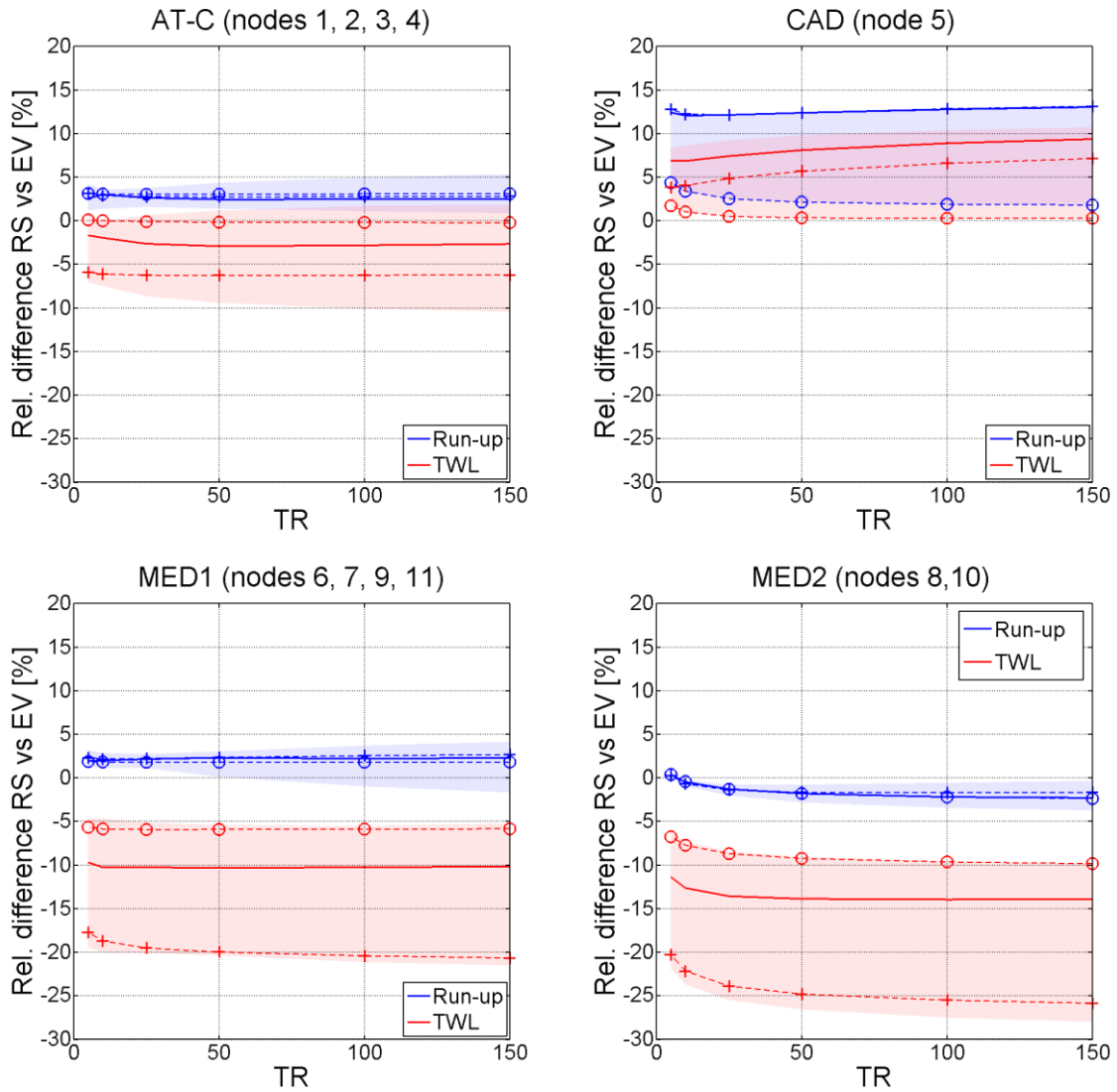


Figure 6. Differences between approaches in run-up (Ru) and total water level (TWL). The solid line represents the median of the corresponding variable from all data nodes and beach slopes. The shaded area represents the 95% probability range. Dashed lines represent average results at $\tan\beta = 0.025$ (cross) and $\tan\beta = 0.20$ (circle).

The general behaviour is an underestimation of Ru by the EV approach except for the locations of MED2 where the RS approach provided values $\sim 0-5\%$ lower than the EV one. Averaged Ru differences for dissipative ($\tan\beta = 0.025$) and reflective ($\tan\beta = 0.20$) profiles are nearly identical to the median, except for CAD, where differences in

dissipative and intermediate slopes (~12%) are higher than in reflective profiles (~0-4%).

When the surge is added to R_u to obtain TWL at the beach, a switch towards overestimation by the EV approach is observed (Figure 6). This result is expected due to the adopted approach to combine both components.

The differences between both methods will depend on the previous differences in R_u and the local dependencies between waves and surge. Thus, at Mediterranean clusters, using the EV approach results in overestimation, with median between 10% and 15%. These differences are significantly higher for dissipative beaches (~20-25%) than for reflective (~5-10%), because the relative contribution of surge to TWL is higher (smaller R_u). The only exception is CAD, where intermediate slopes induce the largest differences. At the AT-C cluster, results also show an underestimation of the EV approach, although of smaller magnitude because of the smaller contribution of S_U to the TWL. The exception is the node 5 where TWL values obtained by applying RS are larger. This change in behaviour is associated with the fact that this node presented the largest underestimation by the EV method in R_u values. The addition of the S_U to obtain the TWL has a lower impact in CAD and AT-C than in MED1 and MED2.

Water Volume estimators

Figure 7 shows obtained differences for overtopping discharge at the peak of the storm along the Spanish coast. The first aspect to be highlighted is that the differences and their variability significantly increase due to the properties of eq.4. This is illustrated in Figure 4, c-d where it can be seen that Q and TWV extreme distributions show a different shape for the EV and RS approaches.

The results mimic the ones obtained for the TWL although with larger magnitudes. Thus, at MED1 and MED2, results show an overestimation of Q by the EV approach. The differences increase with TR reaching values up to 120% for TR of 150 yr. As for TWL, AT-C shows a similar response than the observed in the Mediterranean but of lower magnitude, with maximum differences up to 40% for TR of 150 yr. On the other hand, results for the CAD node show larger values of Q when using the RS method and lower variability than in other locations. In this case, the differences slightly decrease with TR, reaching values of ~50-60% for TR between 100 and 150 yr.

When Q values are integrated over storm duration to obtain TWV, the calculated differences show the same behaviour than observed for Q (Figure 8). The magnitude of computed differences significantly increases at those clusters showing an overestimation of the EV method (i.e. AT-C, MED1 and MED2), reaching up to ~550% for TR of 150 yr. In the CAD node, the previously observed under-prediction by the RS method is reproduced for low-medium TR (10 to 50 yr) and switches towards over-prediction reaching ~25% for TR of 150 yr.

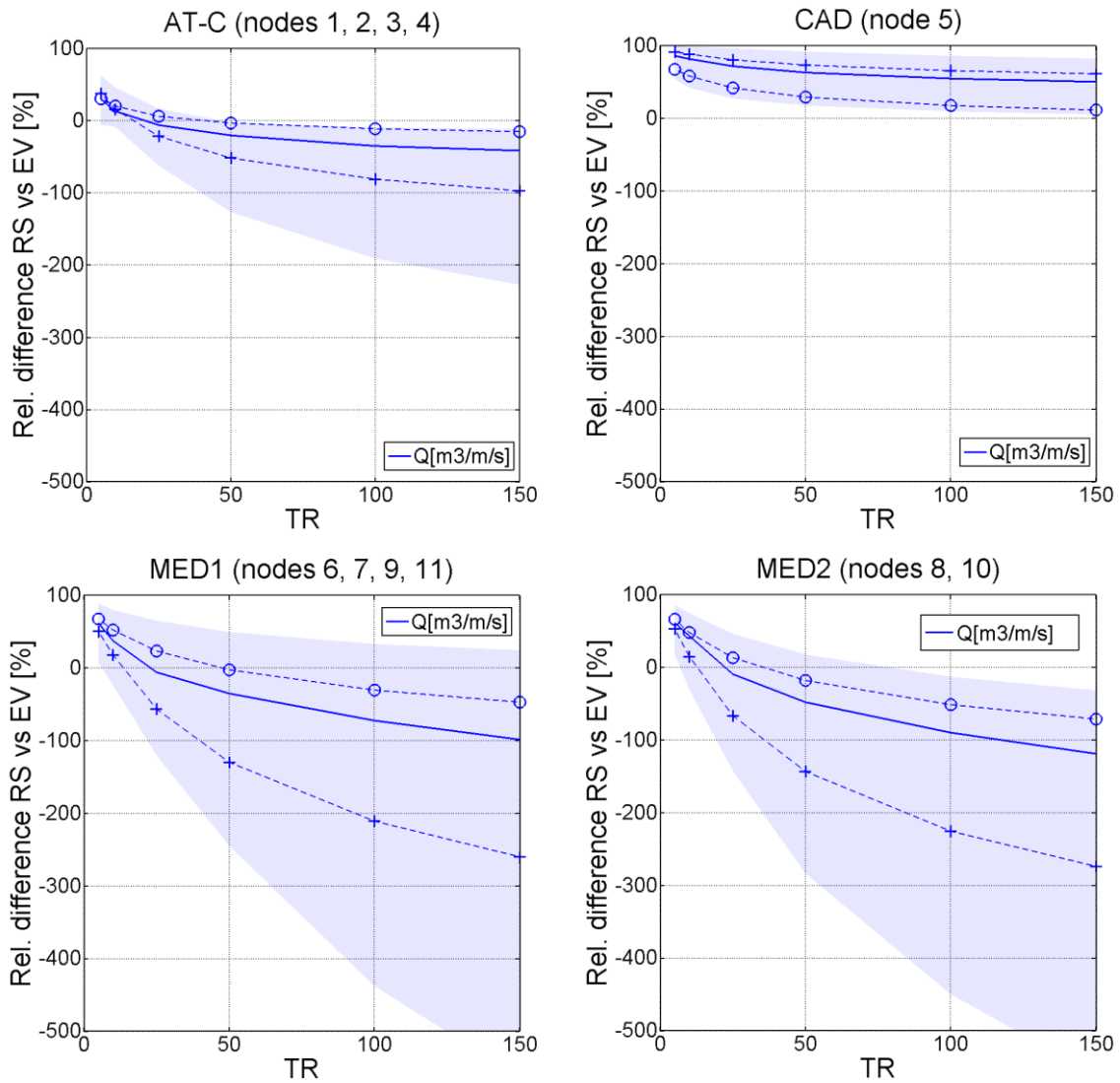


Figure 7. Differences between approaches in overtopping (Q). The solid line represents the median from all of the data nodes and beach slopes-heights within groups. The shaded area represents the 95% probability range. The dashed lines represent average results at $\tan\beta = 0.075$ (cross) and $\tan\beta = 0.20$ (circle).

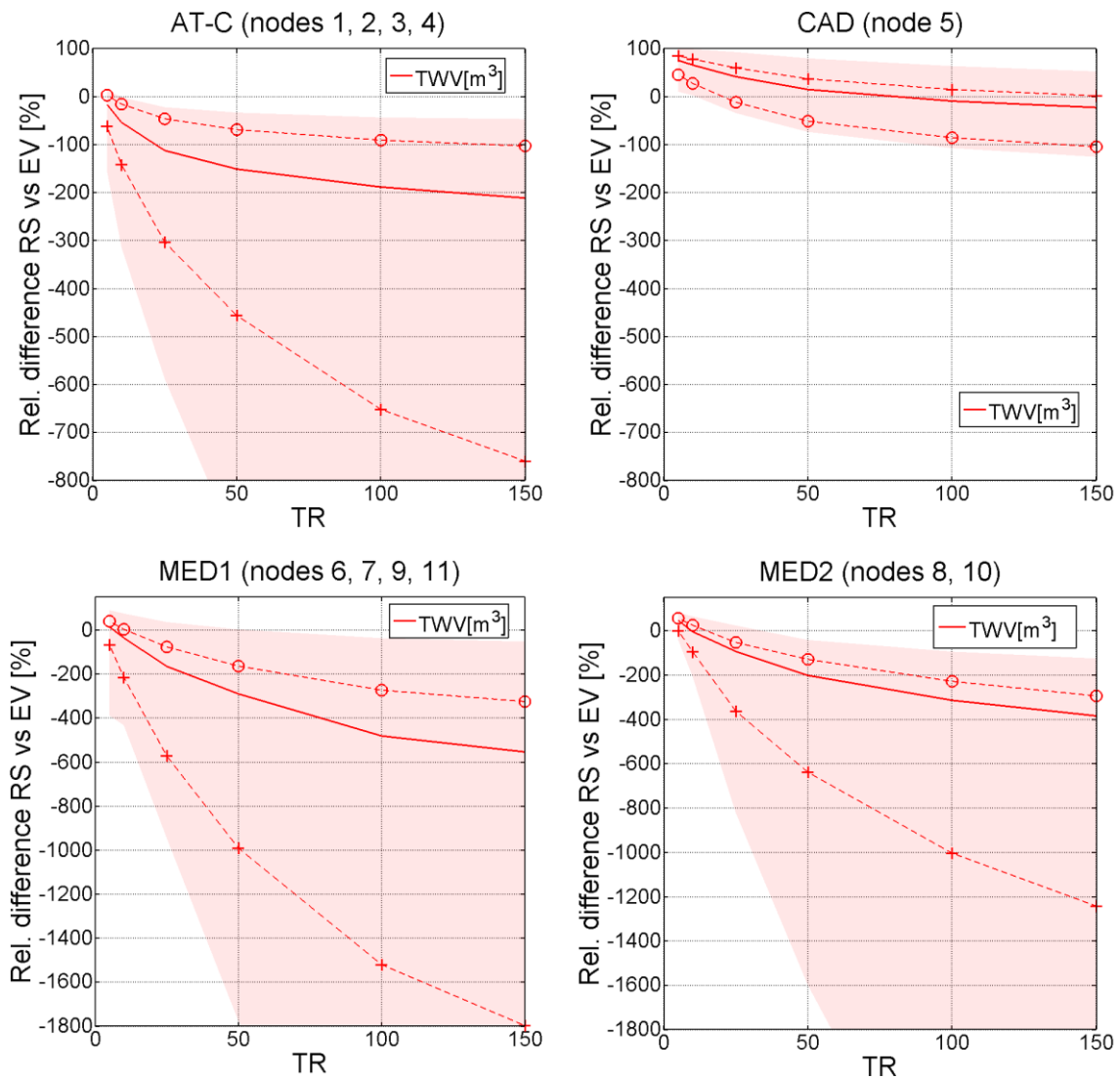


Figure 8. Differences between approaches in total water volume (TWV). The solid line represents the median from all of the data nodes and beach slopes-heights within the groups. The shaded area represents the 95% probability range. The dashed lines represent average results at $\tan\beta= 0.075$ (cross) and $\tan\beta= 0.20$ (circle). Note that y-axis scale is different between upper and lower graphs.

Inundation map estimation

Finally, to illustrate how the differences shown above can propagate to the final step in most of flood hazard assessments, the flood-prone area has been calculated for each cluster under identical conditions of TR, beach morphology (slope of 0.1 and beach

height of 2 m) and topography. TWV results for the 100 yr TR are averaged (Table 3) and then used as boundary conditions to model inundation with LISFLOOD-FP.

The application of both EV and RS approaches leads to the inundation maps shown in Figure 9 and the corresponding inundated areas (Table 3).

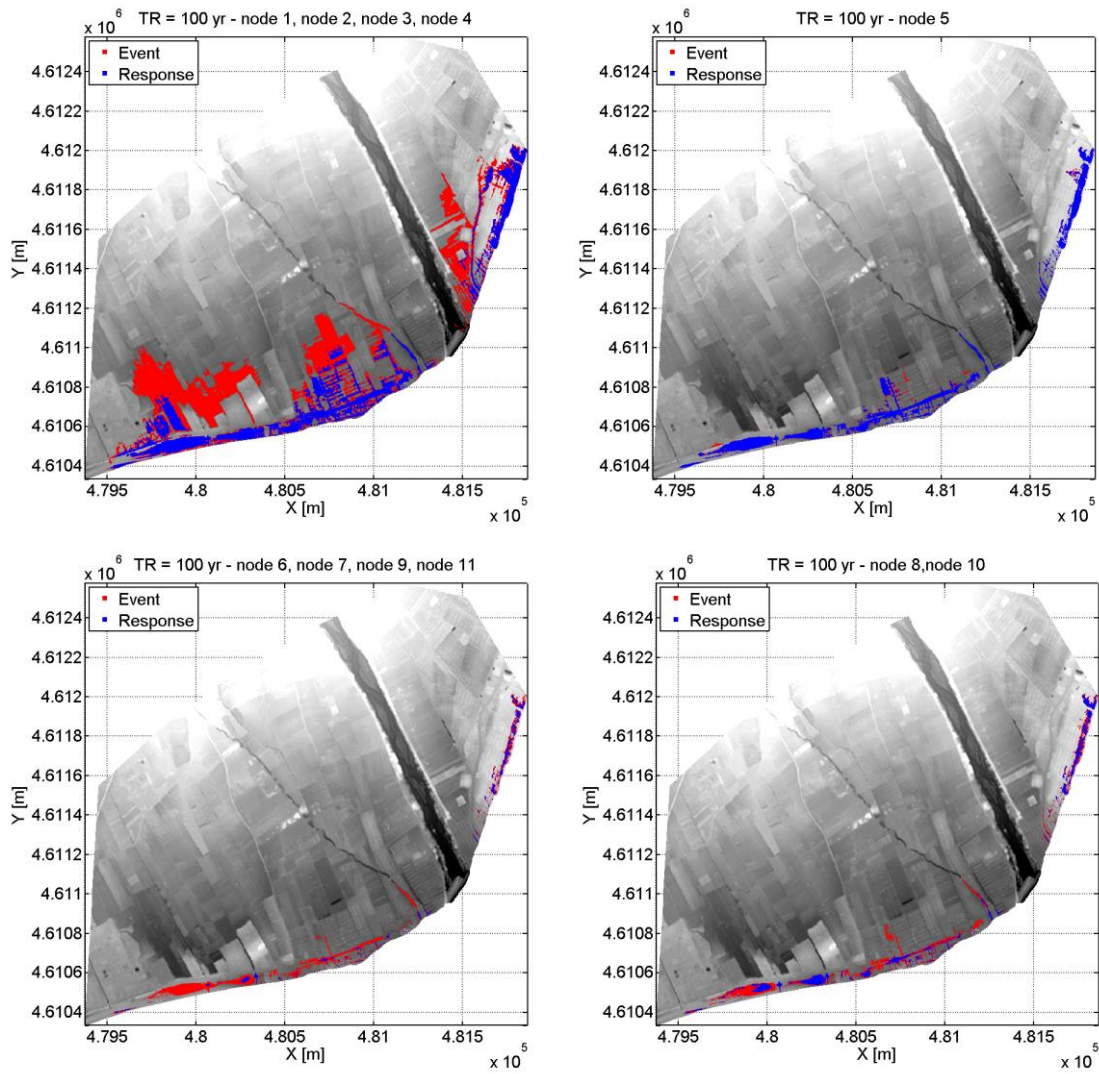


Figure 9. Inundation TR= 100 yr maps simulated for beach slope 0.1 and height 2 m over the Tordera Delta floodplain.

The results show, as expected, higher inundation differences in those cases where TWV differences were also greater. The divergence between EV and RS in terms of inundated area depends on the morphology of the hinterland and the absolute magnitude of the TWV, which is significantly higher for Atlantic-Cantabric hydrodynamics than for Mediterranean conditions for the same beach morphology. The simulated scenarios illustrate different examples of what can be expected in inundation estimation regarding the choice between the EV and RS. For the simulated low-lying floodplain, a high TWV magnitude implies a large inundated area. AT-C (nodes 1 to 4) shows a 112% overestimation of EV in inundation given a TWV difference of 740% at the boundary. Lower TWV provides increasingly shorter inundation surfaces. Mediterranean locations (nodes 6 to 11) show between 75% and 123% EV overestimation, whereas differences were 3 to 5 time larger for the TWV at the boundary. CAD (node 5) presents low differences in both TWV and inundated surface (5 and 9% respectively, Table 3).

In other words, the difference in the inundated area is proportional to the relative difference in TWV but highly modulated by the absolute magnitude of the TWV and the shape of the hinterland.

Table 3. Synthesis of inundation map results. Total water volume entering the hinterland and inundated surface calculated with the event and response approaches for TR= 100 yr, slope= 0.1 and freeboard= 2 m.

Variable	Case	Response	Event	Diff% (eq. 6)
TWV	AT-C	152.420	1.279.800	-739,7%
[m ³]	CAD	121.090	127.910	-5.6%

	MED1	7.924	36.031	-354.7%
	MED2	18.527	105.080	-467.2%
INUNDATED AREA [Ha]	AT-C	26.68	56.16	-111%
	CAD	15.34	16.70	-9%
	MED1	4.99	11.12	-123%
	MED2	7.64	13.34	-75%

DISCUSSION

In this work differences resulting from the method to assign probabilities to inundation hazard estimators have been assessed. To this end, the use of the event and response approaches along the Spanish coast has been compared, in order to cover different wave and water level climates.

The obtained results highlight the existence of differences between the approaches. The choice of the method, which is usually driven by data availability, can be a significant source of uncertainty in the inundation hazard assessment.

The magnitude of the differences depends on the location where the assessment is performed since this determines the exposure to wave and water level conditions. The clustering analysis permitted identification of locations with similar differences in applying both methods. Thus, the results suggest the existence of two homogeneous areas along the Spanish coast with a differentiated behaviour, the Atlantic-Cantabric and the Mediterranean. This result reflects that differences in wave and water level climates not only affect the magnitude of induced hazard but also the expected uncertainty to assess their probability of occurrence. In addition to this big spatial division, two

subgroups per area were also identified in terms of the quantified differences between methods in run up and total water level probability distributions.

The locations with higher differences when using Ru as hazard estimator can be related with high scatter of the Hs-Tp variables and thus with high variability (Figure 10). When assessing TWL, the correlation between SU and Ru is key to how the differences between approaches will propagate. To assess the incidence of this correlation, the Spearman Rho was used (see e.g., Genest and Favre, 2007). Notably, node 5 showed a singular behaviour for both Ru and TWL (Figure 6) and it has a high positive Hs-Tp scatter and the largest positive correlation in terms of Spearman Rho between Ru and SU (Figure 10). In contrast, the Mediterranean locations with larger overestimation of TWL with the EV method present negative values of the Spearman Rho correlation coefficient. This should indicate that, in such places, the assumption of adding SU and Ru with a certain return level and obtaining a TWL with that same probability is less realistic, specially under conditions where SU mainly dominates the TWL, e.g. in dissipative conditions.

When calculating TWV, both the estimation of the duration of the event and the hypothesis about its shape introduces new assumptions in the event approach which lead to the increase of differences between methods. Locations showing a larger scatter of Hs-Dur (AT-C and CAD, Figure 10) also concurrently show lower differences between the event and response in TWV (Figure 8). Although these nodes also showed lower differences in Q (Figure 7), compared to the Mediterranean locations, their relative increase from Q to TWV is also smaller. Thus, this may also suggest that the errors introduced by the assumption of the triangular shape of the storm evolution in time have a deeper impact.

accordance with the observations of Divoky and McDougal, 2006. When assessing the Q and TWV variables, the uncertainty due to the extreme value analysis is also larger, as denoted by a poorer fit by the GPD distributions. Closer attention to this aspect would allow better isolation of this component from the obtained results.

Thus, the event approach is only recommended for large-scale, less-detailed assessments (e.g., Stockdon et al 2007, Armaroli and Duo, 2018) where the target variable may be R_u or eventually TWL if the surge and waves are sufficiently correlated.

Results for TWV and inundated surface showed that differences between methods increase beyond an admissible range with large variability depending on the magnitude of the forcing and beach morphology. This implies that uncertainties are so large that many scenarios can be observed for the same return period: (i) large TWV differences with a large absolute TWV led to a large inundation extent and high differences (over 100% in the inundated area); (ii) similar TWV estimations with medium-large absolute magnitudes led to comparable inundation maps (a difference lower than 10%), but this was only observed in one out of 11 analysed nodes; and (iii) a large difference in TWV with medium-low absolute magnitudes led to a small inundation extent with high differences, which means that one of the approaches may cause a damaging inundation while the other may not cause any flooding beyond the beach itself. These different cases lead to different misleading conclusions in inundation risk assessment and, then, in decision making for coastal management. Thus, if the inundation assessment needs to be more detailed and in a smaller scale with the aim of obtaining discharges or inundation maps (e.g., Chini et al. 2012; Prime et.al 2016), the response approach would be preferable since errors introduced by the event approach may no longer be admissible.

CONCLUSIONS

The event and response approaches to assign probabilities to the intensity of the inundation hazard were compared at 11 locations covering all wave and water level climates around Spain. The magnitude of the differences between methods is location-dependent. Similarities in wave and water level climates influence not only the magnitude of the hazard but also the uncertainty when obtaining their probability of occurrence. Notably, the results highlight that overall relative differences between approaches are higher at the Mediterranean Spanish basin than in the Atlantic and Cantabric locations, due to a milder climate with weak correlation between waves and water levels in the Mediterranean.

Although the response approach is the direct way to obtain the probability of occurrence of coastal inundation hazards due to the multivariate dependence of involved variables, if data availability forces the application of the event approach for inundation assessments, the run-up or total water level (with good correlation between waves and surge) distributions reasonably approximate those of the response approach with lower associated uncertainty. If the inundation assessment aims to create an output for overtopping discharges or inundation maps, observed errors of the event approach suggest that it would produce misleading conclusions in inundation-related coastal management and decision-making.

Thus, the differences between approaches also depend on the estimator used to assess the inundation hazard. The performance of the event approach worsens as the estimator is closer to the inundation maps, where simplifications in the duration and assumptions on the shape of the storm have a great impact. The results indicate that the choice of the

method, which is usually driven by data availability, is an important source of uncertainty in the inundation hazard assessment.

Acknowledgements

This work has been done in the framework of the M-CostAdapt (CTM2017-83655-C2-1-R) and CODA-RETOS (MTM2015-65016-C2-2-R) research projects, funded by the Spanish Ministry of Economy and Competitiveness (MINECO/AEI/FEDER, UE), and by the Secretaria d'Universitats i Recerca del Departament d'Economia i Coneixement de la Generalitat de Catalunya (2017SGR773). The first author was supported by a PhD grant from the Spanish Ministry of Education, Culture and Sport. Authors thank to the Institut Cartogràfic i Geològic de Catalunya for supplying Lidar data used in this study.

References

- Apel, H., Thielen, A.H., Merz, B., Blöschl, G. (2004) Flood risk assessment and associated uncertainty. *Nat. Hazards Earth Syst. Sci.*, 4, 295-308.
- Arcement, G., Schneider, V., (1989) Guide for selecting Manning's roughness coefficients for natural channel and floodplains. Technical Report WSP2339, U.S. Geological Survey.
- Armaroli, C. and Duo, E., (2018) Validation of the coastal storm risk assessment framework along the Emilia-Romagna coast. *Coast. Eng.*, 134, 159–167, doi:10.1016/J.COASTALENG.2017.08.014.
- Armaroli, C., Ciavola, P., Perini, L., Calabrese, L., Lorito, S., Valentini, A., Masina, M. (2012) Critical storm thresholds for significant morphological changes and damage

- along the Emilia- Romagna coastline, Italy. *Geomorphology* 143-144, 34-51, doi.org/10.1016/j.geomorph.2011.09.006.
- Arns, A., Wahl, T., Haigh, I. D., Jensen, J. and Pattiaratchi, C. (2013) Estimating extreme water level probabilities: A comparison of the direct methods and recommendations for best practise *Coast. Eng.*, 81, 51–66, doi:10.1016/j.coastaleng.2013.07.003.
- Bates, P.D., Dawson, R.J., Hall, J.W., Horritt, M.S., Nicholls, R.J., Wicks, J., Hassan, M.A.A.M., (2005) Simplified two-dimensional numerical modeling of coastal flooding and example applications. *Coast. Eng.*, 52, 793-810.
- Bates, P.D., De Roo, A.P.J., (2000) A simple raster-based model for floodplain inundation simulation. *Journal of Hydrology* 236, 54-77.
- Benavente, J., Del Río, L., Gracia, F.J., Martínez-del-Pozo, J.A., (2006) Coastal flooding hazard related to storms and coastal evolution in Valdelagrana spit (Cadiz Bay Natural Park, SW Spain). *Cont. Shelf Res.*, 26, 1061–1076. <https://doi.org/10.1016/J.CSR.2005.12.015>
- Bosom, E., Jiménez, J.A., (2011) Probabilistic coastal vulnerability assessment to storms at regional scale – application to Catalan beaches (NW Mediterranean). *Nat. Hazards Earth Syst. Sci* 11, 475–484. <https://doi.org/10.5194/nhess-11-475-2011>
- Chini, N. and Stansby, P. K., (2012) Extreme values of coastal wave overtopping accounting for climate change and sea level rise, *Coast. Eng.*, 65, 27–37, doi:10.1016/j.coastaleng.2012.02.009.
- Ciavola, P., Ferreira, O., Haerens, P., Van Koningsveld, M. and Armaroli, C. (2011b) Storm impacts along European coastlines. Part 2: Lessons learned from the MICORE project, *Environ. Sci. Policy*, 14(7), 924–933, doi:10.1016/j.envsci.2011.05.009.

- Ciavola, P., Ferreira, O., Haerens, P., Van Koningsveld, M., Armaroli, C. and Lequeux, Q., (2011a) Storm impacts along European coastlines. Part 1: The joint effort of the MICORE and ConHaz Projects, *Environ. Sci. Policy*, 14(7), 912–923, doi:10.1016/j.envsci.2011.05.011.
- Cid, A., Castanedo, S., Abascal, A. J., Menéndez, M., Medina, R., (2014) A high resolution hindcast of the meteorological sea level component for Southern Europe: the GOS dataset, *Clim Dyn*, 43:2167-2184.
- Coles, S.G., (2001) An introduction to statistical modelling of extreme values. Springer, London.
- Cunge, J.A., Holly, F.M., Verwey, A., (1980) Practical aspects of computational river hydraulics. Pitman Advanced Publishing Program, Boston, 420 p.
- Davison, A.C., Smith, R. L., (1990) Models for exceedances over high thresholds (with discussion). *Journal of the Royal Statistical Society: Series B* 52, 393–442.
- de Moel, H., Asselman, N.E.M., Aerts, J.C.J.H., (2012) Uncertainty and sensitivity analysis of coastal flood damage estimates in the west of the Netherlands. *Nat. Hazards Earth Syst. Sci* 12, 1045-1058.
- Divoky, D., McDougal, W.G. (2006). Response-based coastal flood analysis, Proc.30th Int. Conf. on Coastal Engineering, ASCE, 5291-5301.
- Dupuis, D.J., (1998) Exceedances over high thresholds: a guide to threshold selection. *Extremes* 1 (3), 251–261.
- EC, (2007) Directive 2007/60/EC of the European Parliament and of the Council of 23 October 2007 on the assessment and management of flood risks. *Official Journal of the European Union* L 288 , 06/11/2007, 27-34.

- Egozcue, J. J., Pawlowsky-Glahn, V., Ortego, M. I. and Tolosana-Delgado, R., (2006) The effect of scale in daily precipitation hazard assessment, *Nat. Hazards Earth Syst. Sci.*, 6(3), 459–470, doi:10.5194/nhess-6-459-2006.
- Ferreira, Ó., Plomaritis, T.A., Costas, S., (2017) Process-based indicators to assess storm induced coastal hazards. *Earth-Science Rev.* 173, 159–167. <https://doi.org/10.1016/J.EARSCIREV.2017.07.010>
- Garrity, N.J., Battalio, R., Hawkes, P.J., Roupe, D., (2006) Evaluation of the event and response approaches to estimate the 100-year coastal flood for Pacific coast sheltered waters. *Proc. 30th Int. Conf. on Coastal Engineering, ASCE*, 1651-1663.
- Genest, C., Favre, A-C., (2007) Everything you always wanted to know about copula modeling but were afraid to ask. *Journal of Hydrologic Engineering* 12(4), 347-368.
- Hall, J., Solomatine, D., (2008) A framework for uncertainty analysis in flood risk management decisions. *International Journal of River Basin Management* 6 (2), 85–98.
- Hawkes, P.J., Gouldby, B.P., Tawn, J.A., Owen, M.W. (2002) The joint probability of waves and water levels in coastal engineering design. *Journal of Hydraulic Research*, 40, 241-251. <https://doi.org/10.1080/00221680209499940>
- Hedges, T.S., Reis, M.T., (1998) Random wave overtopping of simple seawalls: a new regression model, *Proc. ICE Water, Maritime and Energy* 130, 1-10.
- Hinkel, J., Lincke, D., Vafeidis, A. T., Perrette, M., Nicholls, R. J., Tol, R. S., ... & Levermann, A. (2014) Coastal flood damage and adaptation costs under 21st century sea-level rise. *Proceedings of the National Academy of Sciences*, 111(9), 3292-3297.
- IPCC (2013): *Climate Change, 2013: The Physical Science Basis. Contribution of Working Group I to the Fifth Assessment Report of the Intergovernmental Panel on*

Climate Change, edited by T. F. Stocker, D. Qin, G.-K. Plattner, M. Tignor, S. K. Allen, J. Boschung, A. Nauels, Y. Xia, V. Bex, and P. M. Midgley, Cambridge University Press, Cambridge, United Kingdom and New York, NY, USA.

IPCC (2012): Managing the risks of extreme events and disasters to advance climate change adaptation. A Special Report of Working Groups I and II of the Intergovernmental Panel on Climate Change, edited by C. B. Field, V. Barros, T. F. Stocker, D. Qin, D. J. Dokken, K. L. Ebi, M. D. Mastrandrea, K. J. Mach, G.-K. Plattner, S. K. Allen, M. Tignor, and P. M. Midgley, Cambridge University Press, Cambridge, UK and New York, NY, USA.

Jiménez, J. A., Sancho-García, A., Bosom, E., Valdemoro, H. I. and Guillén, J. (2012) Storm-induced damages along the Catalan coast (NW Mediterranean) during the period 1958–2008, *Geomorphology*, 143–144, 24–33, doi:10.1016/j.geomorph.2011.07.034, 2012.

Jiménez, J.A., Sanuy, M., Ballesteros, C., Valdemoro, H.I., (2018). The Tordera Delta, a hotspot to storm impacts in the coast northwards of Barcelona (NW Mediterranean). *Coast. Eng.* 134, 148–158. <https://doi.org/10.1016/j.coastaleng.2017.08.012>

Jiménez, J. A., Valdemoro, H. I., Bosom, E., Sánchez-Arcilla, A. and Nicholls, R. J. (2017) Impacts of sea-level rise-induced erosion on the Catalan coast, *Reg. Environ. Chang.*, 17(2), 593–603, doi:10.1007/s10113-016-1052-x.

Jongman, B., Ward, P. J., & Aerts, J. C. (2012) Global exposure to river and coastal flooding: Long term trends and changes. *Global Environmental Change*, 22(4), 823-835.

Laudier, N.A., Thornton, E.B., MacMahan, J., (2011) Measured and modeled wave overtopping on a natural beach. *Coast. Eng.*, 58, 815-825.

- Lin-ye, J., Garcia-Leon, M., Gracia, V., Sanchez-Arcilla, A., (2016) A multivariate statistical model of extreme events: An application to the Catalan coast. *Coast. Eng.* 117, 138–156. <https://doi.org/10.1016/j.coastaleng.2016.08.002>
- Marcos, M., Chust, G., Jordà, G., & Caballero, A. (2012) Effect of sea level extremes on the western Basque coast during the 21st century. *Climate Research*, 51(3), 237-248.
- Masina, M., Lamberti, A., Archetti, R., (2015) Coastal flooding: A copula based approach for estimating the joint probability of water levels and waves. *Coast. Eng.* 97, 37–52. <https://doi.org/10.1016/j.coastaleng.2014.12.010>
- Mather, A., Stretch, D., Garland, G. (2011) Predicting extreme wave run-up on natural beaches for coastal planning and management. *Coast. Eng.* 53(2), 87-109.
- McCall, R. T., Vries, J. S. M. V. T. De, Plant, N. G., Dongeren, A. R. Van, Roelvink, J. A., Thompson, D. M. and Reniers, A. J. H. M. (2010) Two-dimensional time dependent hurricane overwash and erosion modeling at Santa Rosa Island, *Coast. Eng.*, 57(7), 668–683, doi:10.1016/j.coastaleng.2010.02.006.
- Mendoza, E. T., Jimenez, J. A. and Mateo, J. (2011) A coastal storms intensity scale for the Catalan sea (NW Mediterranean), *Nat. Hazards Earth Syst. Sci.*, 11, 2453–2462, doi:10.5194/nhess-11-2453-2011.
- Menéndez, M., García-Díez, M., Fita, L., Fernández, J., Méndez, F. J., Gutiérrez, J. M., (2014) High-resolution sea winds hindcasts over the Mediterranean area, *Clim Dyn*, 42(7-8):1857-1872.
- Poelhekke, L., Jäger, W. S., van Dongeren, A., Plomaritis, T. A., McCall, R. and Ferreira, Ó. (2016) Predicting coastal hazards for sandy coasts with a Bayesian Network, *Coast. Eng.*, 118, 21–34, doi:10.1016/j.coastaleng.2016.08.011.

- Prime, T., Brown, J. M. and Plater, A. J. (2016) Flood inundation uncertainty: The case of a 0.5% annual probability flood event, *Environ. Sci. Policy*, 59, 1–9, doi:10.1016/j.envsci.2016.01.018,.
- Pullen, T., Allsop, N.W.H., Bruce, T., Kortenhaus, A., Schüttrumpf, H., van der Meer, J.W., (2007) *EurOtop. Wave overtopping of sea defences and related structures: Assessment manual* [online]. <http://www.overtopping-manual.com> [accessed october 2018]
- Reguero, B. G., Menéndez, M., Méndez, F. J., Mínguez, R., Losada, I. J., (2012) A Global Ocean wave (GOW) calibrated reanalysis from 1948 onwards, *Coast Eng* 65:38-55.
- Reis, M.T., Hu, K., Hedges, T.S., Mase, H., (2008) A comparison of empirical, semi empirical, and numerical wave overtopping models. *Journal of Coastal Research* 24, 250–262. <https://doi.org/10.2112/05-0592.1>
- Reyes, J. L., Martins, J. T., Benavente, J., Ferreira, O., Gracia, F. J., Alveirinho-Dias, J. M., & López-Aguayo, F. (1999) Gulf of Cadiz beaches: a comparative response to storm events. *Boletín-Instituto Español de Oceanografía*, 15(1/4), 221-228.
- Rodriguez-Ramirez, A., Ruiz, F., Cáceres, L. M., Vidal, J. R., Pino, R., & Muñoz, J. M. (2003) Analysis of the recent storm record in the southwestern Spanish coast: implications for littoral management. *Science of the Total Environment*, 303(3), 189-201.
- Ruggiero, P., Holman, R. A. and Beach, R. A. (2004) Wave run-up on a high-energy dissipative beach, *J. Geophys. Res.*, 109(C6), C06025, doi:10.1029/2003JC002160.
- Sallenger, A.H., (2000) Storm impact scale for Barrier Islands. *Journal of coastal research*, 16(3), pp.890-895.

- Sánchez-Arcilla, A., Mendoza, E.T., Jiménez, J.A., Peña, C., Galofré, J., Novoa, M., (2009) Beach Erosion and Storm Parameters: Uncertainties for the Spanish Mediterranean. *Coast. Eng.* 2008 2352–2362. https://doi.org/10.1142/9789814277426_0194
- Sanuy, M., Duo, E., Jäger, W. S., Ciavola, P., and Jiménez, J. A., (2018) Linking source with consequences of coastal storm impacts for climate change and risk reduction scenarios for Mediterranean sandy beaches, *Nat. Hazards Earth Syst. Sci.*, 18, 1825-1847, <https://doi.org/10.5194/nhess-18-1825-2018>.
- Sayers, P.B., Gouldby, B.P., Simm, J.D., Meadowcroft, I., Hall, J., (2003) Risk, Performance and Uncertainty in Flood and Coastal Defence – A Review. Defra R&D Technical Report FD2302/TR1.
- Stephens, M. A., (1977) Goodness of fit for the extreme value distribution, *Biometrika*, Volume 64, Issue 3, Pages 583–588, <https://doi.org/10.1093/biomet/64.3.583>
- Stockdon, H. F., Sallenger, A. H., Holman, R. A. and Howd, P. A., (2007) A simple model for the spatially-variable coastal response to hurricanes, *Mar. Geol.*, 238(1–4), 1–20, doi:10.1016/J.MARGEO.2006.11.004.
- Stockdon, H.F., Holman, R.A., Howd, P.A., Sallenger, A.H. Jr., (2006) Empirical parameterization of setup, swash and run-up. *Coast. Eng.* 53, 573-588.
- Tarantola, A., (2006) *Elements for physics: Quantities, qualities, and intrinsic theories*, Springer-Verlag, Berlin Heidelberg, doi:10.1007/978-3-540-31107-2.
- Toimil, A., Losada, I. J., Díaz-Simal, P., Izaguirre, C., Camus, P., (2017) Multi-sectoral, high-resolution assessment of climate change consequences of coastal flooding, *Clim Change* 145:431-444.

- Tolman, H., Balasubramanian, B., Burroughs, L., Chalikov, D., Chao, Y., Chen, H., Gerald, V., (2002) Development and implementation of wind generated ocean surface wave models at NCEP. *Weather and Forecasting* 17, 311–333.
- Tomás, A., Méndez, F. J., Medina, R., Jaime, F. F., Higuera, P., Lara, J. L., Ortiz, M. D. and Álvarez de Eulate, M. F. (2016) A methodology to estimate wave-induced coastal flooding hazard maps in Spain, *J. Flood Risk Manag.*, 9(3), 289–305, doi:10.1111/jfr3.12198.
- UNEP/MAP/PAP. (2008) Protocol on Integrated Coastal Zone Management in the Mediterranean. Priority Actions Programme, Split.
- Van Dongeren, A., Ciavola, P., Martinez, G., Viavattene, C., Bogaard, T., Ferreira, O., Higgins, R., McCall, R. (2018) Introduction to RISC-KIT: Resilience-increasing strategies for coasts. *Coastal Engineering* 134, 2-9, doi.org/10.1016/j.coastaleng.2017.10.007.
- Vousdoukas, M. I., Mentaschi, L., Voukouvalas, E., Verlaan, M., Jevrejeva, S., Jackson, L. P., & Feyen, L. (2018) Global probabilistic projections of extreme sea levels show intensification of coastal flood hazard. *Nature communications*, 9(1), 2360.
- Winter, B., Schneeberger, K., Huttenlau, M., Stötter, J. (2018). Sources of uncertainty in a probabilistic flood risk model. *Nat. Hazards* 91, 431–446. <https://doi.org/10.1007/s11069-017-3135-5>.

Figure captions

Figure 1. Locations of wave and surge data used in this work. Data from the Global Ocean Waves (GOW, Reguero et al., 2012) and Global Ocean Surge (GOS, Cid et al 2014) were available for each node.

Figure 2. A flow chart of the steps and their interdependencies in the analysed methods: event (EV) and response (RS). $F_X(TR)$ represents the extreme distribution and $f(H_s)$ the deterministic relationships of a variable with the wave height.

Figure 3. Extreme distributions of H_s (a) and SU (b). T_p vs H_s (c) and duration vs H_s (d) relationships for representative nodes covering the different conditions along the Spanish coast (2-Cantabric, 4-N. Atlantic, 5-S. Atlantic, 6-S. Mediterranean and 10-N. Mediterranean)

Figure 4. Examples of method comparison results for the selected locations (2-Cantabric, 4-N. Atlantic, 5-S. Atlantic, 6-S. Mediterranean and 10-N. Mediterranean) and morphologies (slope = 0.1 and $B = 1.5$). The selected datasets are presented to illustrate the absolute magnitudes of the involved variables at each of the main oceanic fronts.

Figure 5. Dendrogram of the 11 locations based on Euclidean distance in terms of run-up (Ru) and total water level (TWL). Mediterranean locations (MED1 and MED2) are separated from N.Atlantic-Cantabric locations (AT-C) and Gulf of Cadiz (CAD).

Figure 6. Differences between approaches in run-up (Ru) and total water level (TWL). The solid line represents the median of the corresponding variable from all data nodes and beach slopes. The shaded area represents the 95% probability range. Dashed lines represent average results at $\tan\beta = 0.025$ (cross) and $\tan\beta = 0.20$ (circle).

Figure 7. Differences between approaches in overtopping (Q). The solid line represents the median from all of the data nodes and beach slopes-heights within groups. The

shaded area represents the 95% probability range. The dashed lines represent average results at $\tan\beta= 0.075$ (cross) and $\tan\beta= 0.20$ (circle).

Figure 8. Differences between approaches in total water volume (TWV). The solid line represents the median from all of the data nodes and beach slopes-heights within the groups. The shaded area represents the 95% probability range. The dashed lines represent average results at $\tan\beta= 0.075$ (cross) and $\tan\beta= 0.20$ (circle). Note that y-axis scale is different between upper and lower graphs.

Figure 9. Inundation TR= 100 yr maps obtained for beach slope 0.1 and height 2 m over the Tordera Delta floodplain.

Figure 10. Wave height-period-duration scatters (left) and correlation wave height-period and run-up-surge by means of Spearman Rho analysis (right). Double values per node (right) refer to the 2 different Ru formulations in eq.1 and 2.